Ocean Sci. Discuss., 8, 1261–1300, 2011
www.ocean-sci-discuss.net/8/1261/2011/
doi:10.5194/osd-8-1261-2011

Ocean Science
Discussions

Extraction of spatial-temporal rules from mesoscale eddies in the South China Sea Based on rough set theory

Y. Du[1], X. Fan[1], Z. He[2], F. Su[2], C. Zhou[1], H. Mao[2], and D. Wang[2]

[1]State Key Laboratory of Resources and Environmental Information System, Institute of Geographic Science and Natural Resources Research, Chinese Academy of Sciences, Beijing, 100101, China
[2]Key Laboratory of Tropical Marine Environmental Dynamics, South China Sea Institute of Oceanology, Chinese Academy of Sciences, Guangzhou, 510301, China

Received: 29 March 2011 – Accepted: 9 May 2011 – Published: 14 June 2011

Correspondence to: Y. Du (duyy@lreis.ac.cn)

Published by Copernicus Publications on behalf of the European Geosciences Union.

Abstract

In this paper, a rough set theory is introduced to represent spatial-temporal relationships and extract the corresponding rules from typical mesoscale-eddy states in the South China Sea (SCS). Three decision attributes are adopted in this study, which make the approach flexible in retrieving spatial-temporal rules with different features. Spatial-temporal rules of typical states in the SCS are extracted as three decision attributes, which then are confirmed by the previous works. The results demonstrate that this approach is effective in extracting spatial-temporal rules from typical mesoscale-eddy states, and therefore provides a powerful approach to forecasts in the future. Spatial-temporal rules in the SCS indicate that warm eddies following the rules are generally in the southeastern and central SCS around 2000 m isobaths in winter. Their intensity and vorticity are weaker than those of cold eddies. They usually move a shorter distance. By contrast, cold eddies are in 2000 m-deeper regions of the southwestern and northeastern SCS in spring and fall. Their intensity and vorticity are strong. Usually they move a long distance. In winter, a few rules are followed by cold eddies in the northern tip of the basin and southwest of Taiwan Island rather than warm eddies, indicating cold eddies may be well-regulated in the region. Several warm-eddy rules are achieved west of Luzon Island, indicating warm eddies may be well-regulated in the region as well. Otherwise, warm and cold eddies are distributed not only in the jet flow off southern Vietnam induced by intraseasonal wind stress in summer-fall, but also in the northern shallow water, which should be a focus of future study.

1 Introduction

The South China Sea (2°30′–23°30′ N, 99°10′–121°50′ E) is the largest semi-enclosed marginal sea in the northwestern Pacific Ocean, as shown in Fig. 1. It has a large NE-SW oriented abyssal basin with greatest depth 5567 m. There is an approximate 3.5×10^6 km^2 of total area with mean depth of 1212 m. The SCS is well linked to the adjacent seas or oceans through several straits or channels, connecting to the Pacific Ocean through the Luzon Strait, to the Sulu Sea through the Mindoro Strait, to the East

China Sea through the Taiwan Strait and to the Java Sea through the Karimata Strait and so on.

Under the confluence of monsoon forcing, Kuroshio intrusion, and complex topography, the SCS is characterized as an area with strong mesoscale activity (He et al., 2002). Located beneath the East Asian Monsoon system, the SCS has prevailing strong northeast winds in winter (October–next March), and southwest winds in summer (June–August); as a result, the near-surface circulation has an evident feature of seasonal variability (Qu, 2000; Wyrtki, 1961; Xu et al., 1982; Su, 2005). Hence, mesoscale variability shows a seasonal variation of flow pattern. The generation of eddies, as is well known, has a close relationship with wind forcing; positive wind stress curl induces a cyclonic eddy, and negative wind stress curl induces an anticyclonic eddy in the ocean. Sea surface height (SSH) is a useful indicator of upper-layer ocean circulation, being well able to reflect mesoscale signals. Zhuang et al. (2010) conclude that the intraseasonal SSH varibilities are induced by distinct mechanisms on the shelves and in the deep waters of the SCS: barotropic response to intraseasonal wind stress forcing in shallow water, and barotropic and baroclinic instabilities and eddy energy advection in deep water, with an exception offshore from Vietnam in summer.

On the other hand, mesoscale variability also has an interannual variation as a response to El Nino/Southern Oscillation (ENSO) in the SCS. Xiu et al. (2010) reveal that mesoscale eddy activities do not account for the ENSO events directly, although interannual variabilities in SSH fields are highly correlated with ENSO (Xie et al., 2003; Liu et al., 2004; Wu and Chang, 2005; Fang et al., 2006; Wang et al., 2006). Previous works reveal that eddies are shed from strong currents such as the Gulf Stream and Kuroshio (Hurlburt and Thompson, 1980; Li et al., 1998; Hetland et al., 1999), and then generate prominent spatial-temporal variability in regional hydrography (Wu and Chiang, 2007). Observational results show that, in winter, there is an anticyclonic eddy shed from the Kuroshio loop due to an unstable Kuroshio meander in the northern Luzon Strait (Li and Wu, 1989; Jia and Liu, 2004); the eddy subsequently moves westward into the SCS (Li et al., 1998; Wang et al., 2000; Yuan et al., 2006). Direct views of eddy-shedding events can be provided by satellite remote sensing data (Yuan et al., 2007; Li et al., 2002; Su et al., 2002). Numerical studies also support this notion (Yang et al., 2000; Metzger and Hurlburt, 2001) and discuss eddy-shedding mechanisms (Jia et al., 2005). The previous studies reveal that mesoscale eddies propagate westward with a speed of 0.1m/s, the order of magnitude of the phase speed of baroclinic Rossby waves in the SCS (e.g., Wu et al., 2005; Wu and Chiang, 2007; Hwang et al., 2004; Roemmich and Gilson, 2001; Hu et al., 2001; White, 2000; Wang et al., 2008a). Topographic eddy can be induced by an eddy-shedding process resulting from the interaction between unstable rotating fluid and sharp topography in the SCS (Yuan and Wang, 1986; Hu et al., 2001).

Discovery of mesoscale eddies is one of the major breakthroughs in the study of physical oceanography in recent decades, and significantly enhances the understanding of hydrodynamics. Oceanographers pay close attention to the origin, movement and spatial-temporal evolution of local eddies at a specific moment for lack of long-enough time series of data gathered by using hydrographic observation, numerical modeling, remote sensor, and so on. However, there are obvious drawbacks in each approach or technique. Cruise observation is so hard and so expensive, as is well known, that only sparse data can be achieved. Numerical modeling depends on specific boundary conditions heavily, and also intensive computation. Remote sensing is good at extracting instantaneous status rather than continuous process of mesoscale eddies. So it is necessary to introduce a new approach to extract spatial-temporal rules from eddies efficiently, in order to depict their distribution pattern in-depth and quantitatively.

Rough set theory is an approach to extract and represent the knowledge that can be derived from incomplete datasets with uncertainties (Miao and Li, 2008). Since rough set theory is available to analyze data with insufficient and incomplete knowledge, it has been applied in many traditional domains, including finance, medicine, telecommunications, vibration analysis, control theory, signal analysis, pattern recognition, and image analysis (Yasdi, 1996; Polkowski and Skowron, 1998; Polkowski et al., 2000; Skowron, 2001; Leung and Li, 2003). In the present study, rough set theory is introduced to examine spatial-temporal relationships and subsequently extract spatial-temporal rules from mesoscale eddies during November 2003–June 2009 in the SCS. The purpose of this paper is to examine whether the approach is available to extract spatial-temporal rules of mesoscale eddies. In Sect. 2, we present the rough set theory and spatial-temporal relationships representation. Data sources and the spatial-temporal rules of mesoscale eddies in the SCS are described in Sect. 3. The findings are discussed in Sect. 4, followed by a conclusion in Sect. 5.

2 Methods

2.1 Rough set theory

Rough set is a mathematical approach proposed by Pawlak (1982) to extract decision rules from a decision system, which is a special case of an information system. Formally, it can be represented by the form $S = (U, C \cup D)$, where U is a nonempty finite set of objects called the universe, C is a nonempty finite set of attributes and $D \notin C$ is the decision attribute. The elements of C are conditional attributes or simply conditions. The decision attributes may take several values, though binary outcomes are rather frequent (Komorowski et al., 1999). In this study, the universe U may be the whole set of mesoscale-eddy cases in the SCS, and the decision attribute D can be the place of origin, generating season or the type of mesoscale eddies. For example, we can associate the number 1 with a warm eddy, 0 with a cold eddy. Conditional attributes in C are the factors associated with spatial-temporal characteristics of mesoscale eddies, such as intensity, the place of origin, horizontal scale and relationships between a target eddy and its reference eddy[1].

---

[1] Reference eddy is defined as the nearest eddy to target eddy at a specific time. A circular area centered at the target eddy and with a radius of 60 nm was screened to identify the eddy temporally occurring before and spatially closest to the target eddy. This specific eddy is deemed as the reference eddy.

2.1.1 Attribute reducts

Rough set analysis aims at synthesizing an approximation of concepts from acquired data (Bai et al., 2010). There are some concepts that cannot be fully defined in a crisp manner by attributes at hand, e.g., mesoscale ocean eddies cannot be classified by their hydrographic features. Rough sets use upper and lower approximations to describe the uncertain concept.

In rough set theory, attribute reducts is a key step. The basic idea is to retain only the attributes that preserve the indiscernibility relation and the set approximation consequently. The rejected attributes are redundant because their removal cannot worsen the classification. There are usually several such subsets of attributes, and those that are minimal are called reducts (Komorowski et al., 1999).

The decision table is then simplified using the algorithm proposed by Pawlak (1991), which is briefly summarized as follows. The positive region of $D$with respect to C, $\mathrm{POS}_C(D)$ is given by

$$\mathrm{POS}_C(D) = \bigcup_{X \in U/D} \underline{C}X \tag{1}$$

where $\mathrm{POS}_C(D)$ is a collection of all elements in U, which can be uniquely categorized into an equivalence class of D by the partition of a conditional attribute C in the U. X is a subset of $U(X \subseteq U)$ and U/D represents an equivalence class of the decision attributes. CX refers to the lower approximation of X with respect to C.

For an index c in set $C(\forall c \in \underset{\cdot}{C})$, if

$$\mathrm{POS}_C(D) = \mathrm{POS}_{C-\{c\}}(D) \tag{2}$$

then c is dispensable in C with respect to D. If indices in C are all indispensable with respect to D, then C is totally independent with respect to D. Attribute reducts is a process to find a subset of C, which is totally indispensable with respect to D.

Title Page
Abstract Introduction
Conclusions References
Tables Figures
I◀ ▶I
◀ ▶
Back Close
Full Screen / Esc
Printer-friendly Version
Interactive Discussion

2.1.2 Decision rule extraction

Once the reducts is found, the rules are easily constructed by overlaying the reducts over the originating decision table and reading off the values. Let X_i and Y_j be the equivalence classes of *U/C* and *U/D*, respectively. des(X_i) represents the description of equivalence class X_i, that is, the specific values of the conditional attributes in set C. des(Y_j)refers to the description of equivalence class Y_j, that is, the specific values of decision attributes in D. Decision rules then can be generated and expressed as

$$r_{ij}: \mathrm{des}(X_i) \rightarrow \mathrm{des}(Y_j) \qquad Y_j \cap X_i \neq \phi \tag{3}$$

Both the certainty and coverage factors for each specific rule are calculated to determine whether the rule is essential or not (Pawlak, 2001). The certainty factor measures how likely the result (derived from a specific rule) is correct and can be given by

$$\alpha = \left|X_i \cap Y_j\right| / |X_i| \qquad 0 < \alpha < 1 \tag{4}$$

A high value of α for a specific rule indicates that, if the condition attributes satisfy the rules, the decision results are more likely to be correct.

The coverage factor is defined as

$$\beta = \left|X_i \cap Y_j\right| / \left|Y_j\right| \qquad 0 < \beta < 1 \tag{5}$$

which represents, to some extent, the conditional attributes satisfying the rules for a specific result. The value 1 indicates that, for any result, the condition attributes completely satisfy the rules. The lower the value, the lower probability the attributes may observe the rules. The certainty and coverage factors are then calculated for all rules which were generated from the reducts of set C. Only those rules (thereby the corresponding spatial relations) with certainty and coverage factors greater than a preset threshold are accepted.

In the above, it is assumed that the values of attributes are discretised data. If the attribute values are continuous, they should be discretised before hand. Over the years, many discretization algorithms have been proposed and tested to show that discretization has the potential to reduce the amount of data while retaining or even improving predictive accuracy. Current dominant discretization approaches generally fall into 2 categories: non-supervised and supervised. Non-supervised approaches mainly employ equal-frequency and equal-interval algorithms. Supervised approaches mainly employ 1RD, Entropy (MDLP – the minimum description length principle), Naive and Semi-Naive algorithms (Fayyad and Irani, 1992, 1993), which take decision-making information into consideration and have a better discretization effect.

2.2 Application of rough set theory to mesoscale ocean eddies

Considering rough set theory does not need prior information in analyzing data, it can derive a classification or decision rules according to the knowledge reducts procedure. Hence, rough set theory can mine the objective and inherent rules implicit in the data. Given that the dynamic mechanisms of mesoscale eddies are still not grasped completely, our study adapts rough set theory to extract spatial distribution regularities of ocean eddies from high-resolved ocean modeling data in quantity.

The whole process to extract spatial-temporal rules from mesoscale eddies by using rough sets can be divided into three steps (Fig. 2): (1) construct a decision information system based on the data at hand; (2) find minimal reducts of conditional attributes; (3) generate rules according to the reducts.

In the first step, spatial-temporal relationship indices should be transformed from original data, which are then imported into the decision table. This step is crucial when rough set theory is used in spatial analysis of eddies. Many spatial attributes are continuous variables. Under such circumstances, the continuous attributes should be discretized before performing rough set analysis. In our study, a boolean algorithm was chosen to discretize the continuous attributes. It is used to discretise the decision table and a genetic algorithm is then applied to simplify and extract decision rules from mesoscale eddies. In rough set theory, a Boolean reasoning technique is typically applied to solve minimization problems (Skowron, 1995; Skowron and Rauszer, 1991).

Discernibility considerations together with Boolean reasoning could compute minimal, identifying patterns of various kinds. Approaches for discretization based on discernibility are intuitively appealing if used together with discernibility-based data mining approaches (Qhrn, 1999). Nguyen and Skowron (1995) propose such an algorithm-the Boolean reasoning algorithm. In the next step, as is described in Sect. 2.1, finding reducts is used as the attribute selection method. Not all attributes transformed or collected in the first step are the key factors that are related to the decision attribute. So it is important to select attributes that are in close relation to the decision. Finally, spatial-temporal relationship rules of eddies in the SCS are generated from the two reducts by overlaying the reducts over the originating decision table and reading off the values. The certainty and coverage factors of each specific rule are then calculated (Wang, 2001).

We present the detailed procedures to represent spatial-temporal relationships of mesoscale eddies, in view of the importance of the first step. As illustrated in Fig. 3, the procedures as follows:

1. Identify and select spatial-temporal relationships among eddies based on prior knowledge. For example, the distance between the target eddy and the nearest one which is generated most recently or distance between the target eddy and the mainland coastline that can be selected as a specific relationship for investigation.
2. These relationships ware then described by a series of quantitative indices. For example, the RCC-8 model (Randell et al., 1992; Randell and Cohn, 1989) can be used to describe the topological relationship among eddies.
3. Decision tables are constructed with each row representing a case of an eddy, while columns record condition and decision attributes. The values in each row, except for the decision attributes, are the quantitative indices which are derived from spatial-temporal relationships.

According to the previous studies, two types of attributes of eddies are considered in this paper. One is their own characteristic attributes. Another is features of spatial-temporal relationships, including:

1. Place of origin (Zone). According to generating mechanisms of mesoscale eddies, the SCS is divided into 4 zones: northeastern, central, southeastern, and southwestern zones (Wang, 2004), as shown in Fig. 1.
2. Generating season (Time). Spring is from March to May, summer from June to August, fall from September to November, and winter from December to next February.
3. Type of eddy (Type): warm or cold eddy.
4. Intensity of eddy M (Intensity): SSH difference in metres between the center and the periphery of an eddy.
5. Vorticity (Vorticity) with an approximation of the relative vorticity of a eddy:

$$\varsigma = \frac{\partial v}{\partial x} - \frac{\partial u}{\partial y} \approx \frac{8gM}{fD^2} \quad (6)$$

where ς is eddy's vorticity in s^{-1}, M eddy's intensity, D eddy's diameter. The Coriolis parameter f is $10^{-4}\,\text{s}^{-1}$, and the acceleration of gravity g is $9.80\,\text{m}\,\text{s}^{-2}$.

1. Horizontal scale of the eddy (HorizontalScale) in metres: the average of the major axis and the minor axis of an enclosing ellipse.
2. Temperature at the center of an eddy (CentralTemp) in Celsius degree.
3. Difference of temperature between the center and the periphery of an eddy (TempDiff) in Celsius degree.
4. Mean depth (Depth) in metres: the average water depth at the center of an eddy.

5. The Euclidean distance (Distance) in metres from the geometric center of a target eddy to its reference eddy.
6. Directional relationship (Direction) to the reference eddy. In all eight directions are considered, involving north (N), northeast (NE), east (E), southeast (SE), south (S), southwest (SW), west (W) and northwest (NW).
7. Topological relationship (Topology) to the reference eddy, which can be represented by the RCC-8 Model (Randell et al., 1992; Randell and Cohn, 1989) as disjoint or overlapping.

3 Results

3.1 Data

Raw data can be acquired from output of the US Naval Research Laboratory (NRL, http://www7320.nrlssc.navy.mil/global_nlom32/scs.html) NLOM (the NRL Layered Global Ocean Model), including SSH, SST and surface current speed. The SSH data is assimilated from satellite data acquired by ENVISAT, GFO and JASON-1, etc. The SST data is assimilated from IR data with a temporal resolution of 1 day and a horizontal spatial resolution of $(1/32)^\circ \times (1/32)^\circ$. The SCS is divided as 4 zones ($Z_1 - Z_4$, shown in Fig. 1), according to generating mechanisms of mesoscale eddies (Wang, 2004). We identify eddies in the SCS and track their evolution process from 5-year-and-8-month time series of SSH data during November 2003–June 2009 in accordance with the following four criteria:

1. There exist closed SSH contours (Wang et al., 2003; Lin et al., 2007).
2. The horizontal scale is not less than 100 km (Wang et al., 2003; Lin et al., 2007).
3. The eddy can be tracked over 20 days.
4. The SSH difference between center of an eddy and its outmost contour, intensity of an eddy M, is not less than 8 cm (Lin et al., 2007).

Wang et al. (2003) choose 30 days as the minimal lifetime of eddy processes, and 5 weeks in Lin et al. (2007). In this paper, shorter-lifetime eddies are able to be detected, owing to highly resolved raw data. In all 391 typical mesoscale-eddy states, including 291 warm-eddy states and 100 cold-eddy states, are detected in this paper. One of them with the corresponding modeling image is illustrated in Fig. 4a–c.

Initially, reliability of the modeling performance needs to be evaluated by comparing with hydrographic observation. SSHA was obtained from NLOM SSH fields during 2003–2009. AVISO merged temporal 7-day and spatial $(1/12)^\circ \times (1/12)^\circ$ sea level anomaly (SLA) observation is adopted to check the accuracy of NLOM SSHA. In Fig. 5a–e, several deterministic eddies of the SCS are shown, e.g., a warm eddy off the Luzon Strait (marked as red capital A), the eddy pair offshore from Vietnam (red capital D), in summer-fall, and its process of evolution are well reflected in NLOM SSHA. The warm eddy near Xisha Island (red capital C) and the west Luzon eddy (Qu, 2000; red capital B) are also well-reflected in the northern SCS. In addition, a cruise measurement was performed during 16 August –6 September 2008. Hourly current velocity was gathered by using ADCP (supported by South China Sea Institute of Oceanology, Chinese Academy of Sciences, China). Near-sea surface current speeds (38 m beneath) were selected to validate those at the corresponding positions simulated by NLOM. Comparison of the current speeds simulated by NLOM with cruise measurements is shown in Table 1. Accuracy of current speed is calculated as

$$\delta U = \left(1 - \left|\frac{U_{\mathrm{NLOM}} - U_{\mathrm{ADCP}}}{U_{\mathrm{ADCP}}}\right|\right) \times 100\,\% \qquad (7)$$

where U_{NLOM} is the surface current speed simulated by NLOM. U_{ADCP} is the 38 m-layer current speed recorded by ADCP. δU is the ratio of accuracy. δU at 8 (out of 15) stations exceeds 70 %. So we consider the NLOM SSHA acceptable in the SCS.

3.2 Selection of attribute

According to the methodology introduced in Sect. 2, spatial-temporal relationships among mesoscale eddies in the SCS are quantitatively described by the twelve attributes specified in Sect. 2.2. These attributes are first discretised (if continuous) and then imported as condition attributes into a decision table. Decision attributes in each table are selected depending on the specific concerns. So minimal attribute reducts are distinct according to decision attributes. As a result, rules of each issue extracted by rough set theory may be different. The place of origin of each eddy is selected as the decision attribute in Table 2, in order to extract certain rules from spatial-temporal relationships among eddies generated in all 4 zones of the SCS. Generating season is selected as the decision attribute in Table 3 for pursuing the seasonal variation of the rules. And the type of eddies (warm/cold eddy) is selected as the decision attribute in Table 4 when spatial-temporal rules between the two types of eddies are focused on.

In this study the quantitative indices of the twelve attributes depicting 391 typical states of all 76 mesoscale eddies are calculated by a Visual Basic Application (VBA) program running on the ArcGIS platform. The first three indices are used as a decision attribute, the others as condition attributes in decision tables. After constructing the decision table , the Rosetta software (Qhrn, 1999), which is jointly developed by the Department of Computer and Information Science at Norwegian University of Science and Technology and Institute of Mathematics at University of Warsaw in Poland, is used to calculate and extract rules.

3.3 Extraction of spatial-temporal rules of mesoscaleeddies in the SCS

Tables 5–7 show the corresponding spatial-temporal rules extracted from three decision tables (Tables 2–4) in which the decision-making attributes are place of origin, generating season and eddy type, respectively. All the rules have a coverage level of 10 % at least and a certainty level of 100 %, and are arrayed in descending order by the value of coverage level. In all 5 kinds of rules are extracted in Table 5, 11 rules in Table 6, and 13 rules in Table 7, respectively.

The typical eddy-states following all rules in Table 5 are detected and presented in Fig. 6. In all 5 rules are extracted, including 2 rules in zone Z_1 of the SCS, 2 in zone Z_3, and 1 in zone Z_4, respectively. Cold-eddy states following Rule 1 are distributed southwest of Taiwan Island around 2000 m isobaths (zone Z_1). It is obvious that most of the states follow not only Rule 1, but also Rule 2 in this zone, except for two states following Rule 1 merely. In winter, wind stress curl of orographic wind induced by the cordillera on Taiwan Island results in cold water in the subsurface upwelling and creating a cold core eddy due to the Ekman pumping effect (Qu, 2000). In Z_3 zone all the states are in the 4000 m-deeper region of the basin, and follow both Rules 3 and 4 except one state only following Rule 4. There is a warm eddy southwest of Luzon Island besides the famous Luzon Cold Eddy, which is located northwest of Luzon Island. Wang et al. (2008b) reveal that the winter gap winds in the mountainous island chain along the eastern boundary of the SCS are intrinsic regional features of the monsoon due to orographic effects, spinning up cold and warm eddies west of Luzon Island. So, in summer, the eddy pair offshore from Vietnam separated by a wind jet has the same features in horizontal scale and the water depth of eddy core. Figure 6 shows that no rule is extracted in zone Z_2.

Spatial-temporal rules extracted from typical mesoscale eddy states occurring in 4 seasons are presented in Table 6. A total of 8 rules are extracted in winter, 2 in summer, 1 in fall and none in spring, respectively. Spatial distribution of the states following all 11 rules is shown in Fig. 7a in winter, 7b in summer and 7c in fall. No eddy state is extracted in spring. As Fig. 7a presents, all the states, in winter, are concentrated around the western 2000 m isobaths of the northern basin (both zones Z_1 and Z_2) with an exception of one state in the basin center (zone Z_3). There are many more states of eddies in winter than the other seasons.

In Fig. 7a, two states obey Rules 1 and 2 together in zone Z_2. Another two obey Rules 2 and 3 together in zone Z_2. These four states locate in the eastern Xisha Island, maybe originating from the Xisha Warm Eddy AE1 in Wang et al. (2008a). Two states obey Rules 6 and 7 together: one lies in zone Z_1, another in zone Z_2. Furthermore, several eddy states obey three rules simultaneously, including two obeying Rules 1, 6 and 7 together in zone Z_2, which maybe originates from the Xisha Warm Eddy AE1 detected by Wang et al. (2008a), and three obey Rules 2, 6 and 7 together in zone Z_2, on the boundary between zones Z_1 and Z_2, which maybe originates from another Xisha Warm Eddy AE2 detected by Wang et al. (2008a). Three states obey Rules 4 and 8 together in zone Z_1. In winter, the Kuroshio intrusion plays a major role in them (e.g., Su, 2004; Wu and Chiang, 2007; Zhuang et al., 2010). Frontal instability at the Kuroshio intrusion could be one mechanism in eddy shedding (Wang et al., 2000; Su, 2004). In addition, four obey Rules 2, 3 and 8 together in zone Z_2, and two states obey four rules (Rules 1, 3, 6 and 7) together in zone Z_2. The six states are too close to detect clearly whether they originate from Xisha warm eddy processes.

In summer, the number of typical states decreases obviously in Table 6. Most of the states, as shown in Fig. 7b, are around the western 2000 m isobaths with one exception in the central basin (zone Z_3). There are two clusters of states off the Vietnam coast, eight states over the shelf of northern Vietnam (<2000 m), and seven in the 2000 m-deeper region off southern Vietnam in zone Z_4. Only two obey both rules at the same time, one is in shallow water off northern Vietnam coast, the other is in deep water off southern Vietnam Peninsula. Besides, there are three warm-eddy states locate in north of the basin, the boundary of zones Z_1 and Z_2. Several studies show that, off central Vietnam, there is a cyclonic gyre north of about 12° N, but an anti-cyclonic gyre to the south (Kuo et al., 2000; Xie et al., 2003). Associated with these gyres is a northward orographic wind jet turning offshore from the Vietnam coast near 12° N. The typical warm-eddy states are distributed not only on south of the jet flow induced by intraseasonal wind stress, but also on the northern shallow water; it is unclear how the eddy is generated and should be a focus of future study. We have to note the wind jet flow simulated by NLOM northwards up to 13°–14° N, so the two clusters are distributed on both sides along 14° N.

In fall, in all ten eddy states are around the western boundary of 2000 m isobaths of the northern basin (zone Z_2) exclusively, as shown in Fig. 7c, one half in north of the zone, the other half in the south. This is the least in number among the four seasons. These states gather as four clusters. Two are off west Luzon Strait, another two are off the southeast of Hainan Island. Both the two clusters composed by 4 states seem to derive from the warm eddy AE1 and AE2 near Xisha Island in Wang et al. (2008a).

Spatial-temporal rules extracted from two types of typical eddy states (warm/cold eddy) are shown in Table 7. A total of 6 rules (Rules 1, 2, 4, 5, 9 and 11) are extracted for warm-eddy states, and 7 rules (Rules 3, 6, 7, 8, 10, 12 and 13) for cold-eddy states. Figure 8 shows spatial distribution of cold-eddy states in 8a and warm-eddy states in 8b.

All cold-eddy states are distributed as a band along the western 2000 m isobaths (Fig. 8a) from west of Luzon Strait to the southeast of Hainan Island, and to offshore of Vietnam; they are also revealed recently by both model and satellite data (Xiu et al., 2010). In zone Z_1 two cold-eddy states obey Rules 7 and 13 together in spring, five obey Rules 7 and 8 together in fall and two obey Rules 12 and 13 together in spring. Besides, one cold-eddy state obeys Rules 7, 8 and 10 together in fall. All of them occur in spring and fall, neither summer nor winter, and they converge on the northern tip of the basin and west of Luzon Strait, as shown in Fig. 8a; they are induced by wind stress curl resulting from the blockage effect of Cordillera on the southwest of Taiwan Island (Qu, 2000; Su, 2004) or the net water transport into the SCS via the Luzon strait (Su, 2004). Figure 8a also indicates that states following Rule 3 seldom exist southwest of Taiwan Island. Lack of a cold-eddy rule in winter, may result from the rules' coverage level being less than 10 %, not indicative of no cold eddy at all. In zone Z_2 one cold-eddy state obeys Rules 7 and 13 at the same time. Three obey Rule 13 in spring, and one obeys Rule 12. There are none in zone Z_3. In zone Z_4, two clusters of states are separated by the wind jet along 13°–14° N. Four cold-eddy states following Rule 12 are located at the northern wind jet. Six cold-eddy states follow Rules 6 and 8 together in fall, distributed on each side of the jet as parts of the two clusters, respectively. And one state follows Rules 6, 8 and 10 together in fall, also on the southern jet. In this zone, the cold-eddy states located at both northern and southern sides of the Vietnam jet flow only occur in fall. Wind forcing plays a major role in their generation (Zhuang et al., 2010). Four cold-eddy states obey Rules 6 and 13 together in spring, located only on the southern wind jet off the Vietnam coast. It is unclear why a cold eddy occurs in this season, and no previous study focuses on this. Oceanologists should pay more attention to this phenomenon in future study.

Figure 8b shows that typical warm-eddy states are predominant in quantity, and distributed as two strips: one is around the western 2000 m isobaths, another is NE-SW in the deeper region of the abyssal basin west of Luzon Island, in good agreement with the spatial pattern achieved by both model and satellite observations (Xiu et al., 2010) and total eddy energy achieved by the intraseasonal variability of SSH (Zhuang et al., 2010). They occupy all 4 zones of the SCS, especially in the south. Rule 1 reveals general features of numerous warm-eddy states in the SCS, which are distributed predominantly offshore from Vietnam and west of Luzon Island. Most of states obeying Rule 4 occur in north of western 2000 m isobaths. In winter the Kuroshio intrusion induces the generation and evolution of mesoscale eddies west of Luzon Strait, and the Dongsha warm current induces frontal warm eddies (Su, 2004) near Dongsha Island. The others are southwest of Luzon Island, named the West Luzon Eddy by Qu (2000). Wind forcing converges on the upper-layer warm water and downwelling under the Ekman pumping effect (Qu, 2000). Downwelling brings warm water from surface to the deep creating warm core eddies. Several warm-eddy states obey Rules 1 and 9 together. One is located in zone Z_1, the others in zones Z_2–Z_4. Two states obey Rule 1 together with Rule 11. One is in zone Z_1, the other in zone Z_2. Furthermore, in zone Z_2, two states obey Rules 1 and 5, and several obey Rules 1, 9 and 11 simultaneously. In zone Z_3 several states obey Rules 4 and 5 together, and two obey Rules 1, 5 and 9 together. Two obey Rules 1, 2 and 9 together in zone Z_4. Eddies off southwestern Luzon Island, following Rules 1, 4 and 5, are considered to be induced by the interaction between strong barotropic shelf currents and the local topography (Xiu et al., 2010). There is no warm-eddy state in the northern tip of 2000 m isobaths (southwest of Taiwan Island or west of Luzon Strait), as is clear in Fig. 8a, maybe due to lack of negative wind stress curl.

There is a phenomenon that some typical mesoscale-eddy states follow two rules or more in Figs. 6–8, respectively, indicating they have much stronger regularity in spatial-temporal distribution. From the above analysis, we find that, typical cold-eddy states, located southwest of Taiwan Island, the northeastern tip of the basin, occurred in winter (Fig. 6). Typical warm-eddy states are distributed either southwest of Luzon Island, the deepest region of the basin, or the western edge of 2000m isobaths. It is shown in Table 6 that no rule can be co-followed by the two types of eddies.

4 Discussion

Lots of previous works on mesoscale eddies in the SCS have been performed by in situ measurements, numerical simulation and satellite remote sensing. Some of their conclusions can be reproduced in our study, as in the following examples:

1. Through analyzing 5-yr T/P data, Wang et al. (2000) point out that mesoscale eddies in the SCS are active along the western 2000 m isobaths and the NE-SW oriented band from south of Luzon Strait to 11° N around the eastern Vietnam Peninsula. This is also revealed by Lin et al. (2007) through statistical analysis of 10-yr T/P data and Wang (2004) through statistical analysis of 8-yr T/P data. In our study this spatial feature of eddies is confirmed one more time, as shown in Fig. 8b. In this Figure, warm-eddy states are located in the NW-SE oriented band, which confirms the conclusion in Lin et al. (2007) that there are warm eddies in the region (14°–15° N, 118°–120° E) exclusively, but no cold eddy occurs.

2. Cheng et al. (2005) conclude that warm eddies are distributed north of 18° N, which is followed by Rule 1, 2, 5 and 7 in Table 5 and Rule 11 in Table 6. In Fig. 8b, these states are in the western zone Z_2 (18°–20° N).

3. Most mesoscale eddies appear off the eastern Vietnam Peninsula, the western Luzon Strait and in the northeastern SCS, while they are inactive in the southeastern SCS (e.g. Wang, 2004; Lin et al., 2007; Cheng et al., 2005). This is confirmed in Fig. 6.

4. Wang et al. (2008a) examine warm eddies AE1 and AE2 in the northeastern SCS during the winter of 2003–2004. We can confirm that the six states of eddy AE1 in Figs. 2 and 4 of Wang et al. (2008a) follow Rules 1 and 3 together in Table 5 and Rules 4 and 11 together in Table 6, while none of rules is followed by states of eddy AE2. AE2 locates in zone Z_1, as shown in Fig. 6. No rule can be extracted among warm-eddy states in this zone in winter other than Rule 1 of Table 6. It should be pointed out that we are not able to obtain the Euclidean distance, directional relationship and topological relationship of the two eddies. Thus only some of rules in Tables 4–6 could be confirmed by Wang et al. (2008a).

However, there are several features achieved in our study that were not presented in previous works. In winter, warm eddies, as is well known, are generated in the northeastern SCS resulting from the frequent Kuroshio intrusion, thus most oceanographers pay close attention to their generating mechanisms, processes of evolution, and so on. Whereas, a few rules extracted in this zone are followed by cold eddies in winter, indicating cold eddies may be well-regulated in the region. Meanwhile, west of Luzon Island, the famous Luzon cold eddy is focused. Several rules, however, are achieved for warm eddies in this zone, indicating warm eddies may be well-regulated in the region as well. Otherwise, warm eddies are distributed not only on the jet flow off southern Vietnam induced by intraseasonal wind stress in summer-fall, but also on the northern shallow water, which should be a focus of future study. Similarly, cold eddies are also located at both northern and southern sides of the Vietnam jet flow in fall. And there are cold eddies generated off southern Vietnam in spring. These are interesting, and will be paid attention.

5 Conclusions

In this paper, a rough set theory is introduced to represent spatial-temporal relationships and extract the corresponding rules from typical mesoscale-eddy states in the SCS. These rules clearly confirm spatial-temporal distribution patterns and features of these states. Three decision attributes are adopted in this study, which make the approach flexible in retrieving spatial-temporal rules with different features. The results demonstrate that this approach is effective in extracting spatial-temporal rules from typical mesoscale-eddy states. Spatial-temporal rules in the SCS indicate that warm eddies following the rules are generally in the southeastern and central SCS around 2000 m isobaths in winter. Their intensity and vorticity are weaker than those of cold eddies. They usually move a shorter distance. By contrast, cold eddies are in 2000 m-deeper regions of the southwestern and northeastern SCS in spring and fall. Their intensity and vorticity are strong. Usually they move a long distance. In winter, a few rules are followed by cold eddies in the northern tip of the basin and southwest of Taiwan Island rather than warm eddies, indicating cold eddies may be well-regulated in the region. Several warm-eddy rules are achieved west of Luzon Island, indicating warm eddies may be well-regulated in the region as well. Otherwise, warm and cold eddies are distributed not only in the jet flow off southern Vietnam induced by intraseasonal wind stress in summer-fall, but also in the northern shallow water, which should be a focus of future study.

However, the approach requires to select the corresponding spatial-temporal relationships among mesoscale eddies according to each issue. It is also worth noting that the raw data used in this study is derived from numerical modeling. Some of eddies with a shorter life-time or smaller horizontal scale may not be included, as a result of not being identified. So the number of eddies analyzed is fewer than the actual total. In the future, the rough set approach will be improved by supplementing data acquired in different sea areas and seasons into the database, selecting appropriate attribute factors that can better reflect spatial-temporal relationships among eddies, and applying other discretization and reducts algorithms based on rough set theory. Comparison of the results derived from different scenarios would help yield more practically significant rules.

Acknowledgements. This work was fully supported by the National Science Fund (Project No. 41071250), and the National 863 High Technology Programs of China (Project No. 2011BAH23B04), and was granted from the State Key Laboratory of Resource and Environment Information System (Project No. 08R8B500KA). The authors would appreciate comments from reviewers and readers.

References

Bai, H., Ge, Y., Wang, J., and Liao, Y.: Using rough set theory to identify villages affected by birth defects: the example of Heshun, Shanxi, China, Int. J. Geogr. Inf. Sci., 24(4), 559–576, 2010.

Cheng, X., Qi, Y., and Wang, W.: Seasonal and Interannual Variabilities of Mesoscale Eddies in South China Sea, J. Trop. Oceanogr., 24(4), 51–59, 2005.

Fang, G., Chen, H., Wei, Z., Wang, Y., Wang, X., and Li, C.: Trends and interannual variability of the South China Sea surface winds, surface height, and surface temperature in the recent decade, J. Geophys. Res., 111, C11S16, doi:10.1029/2005JC003276, 2006.

Fayyad, U. M. and Irani, K. B.: On the handling of continuous-valued attributes in decision tree generation, Mach. Learn., 8(1), 87–102, 1992.

Fayyad, U. M. and Irani, K. B.: Multi-interval discretization of continuous-valued attributes for classification learning. Proceedings of the 13th International Joint Conference on Artificial Intelligence IJCAI-93. Chambery, France: Morgan Kauffman, 1993.

He, Z., Wang, D., and Hu, J.: Features of eddy kinetic energy and variations of upper circulation in the South China Sea. Acta Oceanol, Sinica, 21(2), 305–314, 2002 (in Chinese with English abstract).

Hetland, R. H., Hsueh, Y., Leben, R. R., and Niiler, P. P.: A loop current-induced jet along the edge of the West Florida shelf, Geophys. Res. Lett., 26(15), 2239–2242, 1999.

Hu, J., Kawamura, H., Hong H., Kobashi, F., and Wang, D.: 3–6 months variation of sea surface height in the South China Sea and its adjacent ocean, J. Oceanogr., 57, 69–78, 2001.

Hurlburt, H. E. and Thompson, J. D.: A numerical study of loop current intrusions and eddy shedding, J. Phys. Oceanogr., 10, 1611–1651, 1980.

Hwang, C., Wu, C. R., and Kao, R.: TOPEX/Poseidon observations of mesoscale eddies over the Subtropical Counter Current: kinematic characteristics of an anticyclonic eddy and a cyclonic eddy, J. Geophys. Res., 109, C08013, doi:10.1029/2003JC002026, 2004.

Jia, Y. and Liu, Q.: Eddy shedding from the Kuroshio bend at Luzon Strait, J. Oceanogr., 60(6), 1063–1069, 2004.

Jia, Y., Liu, Q., and Liu, W.: Primary studies of the mechanism of eddy shedding from the Kuroshio bend in Luzon Strait, J. Oceanogr., 61(6), 1017–1027, 2005.

Komorowski, J., Pawlak, Z., Polkowski, L., and Skowron, A.: Rough sets: A tutorial. Rough fuzzy hybridization: a new trend in decision-making, edited by: Pal, S. and Skowron, A., Singapore: Springer-Vela 3-93, 1999.

Kuo, N. J., Zheng, Q., and Ho, C. R.: Satellite observation of upwelling along the western coast of the South China Sea, Remote Sens. Environ., 74, 463–470, 2000.

Leung, Y. and Li, D.: Maximal consistent block technique for rule acquisition in incomplete information systems, Inf. Sci., 153(1), 85–106, 2003.

Li, L.: A review on mesoscale oceanographical phenomena in the South China Sea, J. Oceanogr. Taiwan, 21(2), 562, 265–274, 2002 (in Chinese with English abstract).

Li, L. and Wu, B.: A Kuroshio loop in South China Sea?, J. Oceanogr. Taiwan, 8, 89–95, 1989 (in Chinese with English abstract).

Li, L., Nowlin Jr., W. D., and Su, J.: Anticyclonic rings from the Kuroshio in the South China Sea, Deep-Sea Res. I, 45, 1469–1482, 1998.

Lin, P., Wang, F., Chen, Y., and Tang, X.: Temporal and spatial variation characteristics on eddies in the South China Sea I. Statistical analyses, Acta Oceanol. Sinica, 29(3), 14–22, 2007.

Liu, Q., Jiang, X., Xie, S., and Liu, W.: A gap in the Indo-Pacific warm pool over the South China Sea in boreal winter: Seasonal development and interannual variability, J. Geophys. Res., 109, C07012, doi:10.1029/2003JC002179, 2004.

Metzger, E. J. and Hurlburt, H. E.: The nondeterministic nature of Kuroshio penetration and eddy shedding in the South China Sea, J. Phys. Oceanogr., 31, 1712–1732, 2001.

Miao, D. and Li, D.: Rough Sets Theory Algorithms and Applications, TsingHua University Press, Beijing, 2008.

Nguyen, H. S. and Skowron, A.: Quantization of real-valued attributes. Proceeding 2nd International Joint Conference on Information Sciences, Wrightsville Beach, NC, 34–37, 1995.

Pawlak, Z.: Rough sets, Int. J. Inform. Comput. Sci., 11(5), 341–356, 1982.

Pawlak, Z.: Rough Sets: Theoretical Aspects of Reasoning about Data, Kluwer Academic Publishers, Boston, 1991.

Pawlak, Z.: Bayes' theorem revised- the rough set view, Proceedings of International Workshop on Rough Set Theory and Granular Computing (RSTGC 2001), Matshue, Shimane, Japan, 1–8, 2001.

Polkowski, L. and Skowron, A.: Rough Sets in Knowledge Discovery 1: Methodology and Applications, 2: Applications, Physica-Verlag, Heidelberg.

Polkowski, L., Tsumoto, S. and Lin, T.: Rough Set Methods and Applications, Physica-Verlag, Heidelberg, 49–88, 2000.

Qhrn, A.: Discernibility and rough sets in medicine: tools and application. Norwegian University of Science and Technology, Norway, 41–51, 1999.

Qu, T.: Upper-layer circulation in the South China Sea, J. Phys. Oceanogr., 30, 1450–1460, 2000.

Randell, D. A. and Cohn, A. G.: Modelling topological and metrical properties in physical processes, Proceedings of the 1st International Conference on the Principles of Knowledge Representation and Reasoning, Morgan Kaufmann Publishers, San Francisco, 55–66, 1989.

Randell, D. A., Cui, Z., and Cohn, A. G.: A spatial logic based on regions and connection. Proceedings of the 3rd International Conference on Principles of Knowledge Representation and Reasoning. Morgan Kaufmann Publishers, San Francisco, 165–176, 1992.

Roemmich, D. and Gilson, J.: Eddy transport of heat and thermocline waters in the North Pacific: a key to interannual/decadal climate variability, J. Phys. Oceanogr., 31, 675–687, 2001.

Skowron, A.: Synthesis of adaptive decision systems from experimental data, Proceedings of the Fifth Scandinavian Conference on Artificial Intelligence, number 28 in Frontiers in Artificial Intelligence and Applications, edited by: Aamodt, A., and Komorowski, J., IOS Press, 220–238, 1995.

Skowron, A.: Rough sets and Boolean reasoning, Granular Computing: An Emerging Paradigm, edited by: Pedrycz, W., Physica-Verlag, Heidelberg, 95–124, 2001.

Skowron, A. and Rauszer, C.: The discernibility matrices and functions in information systems. Intelligent decision support: handbook of applications and advances of the rouogh sets theory, edited by: Słowinski, R., Technical University of Poznan, Poland, 331–362, 1991.

Su, J.: Overview of the South China Sea circulation and its influence on the coastal physical oceanography outside the Pearl River Estuary, Cont. Shelf Res., 24, 1745–1760, 2004.

Su, J., Lu, J., Hou, Y., Fang, G., Wei, Z., and Yin, B.: Analysis of satellite-tracked drifting buoys in the South China Sea, Oceanol. Limnol. Sinica, 33(2), 121–127, 2002 (in Chinese with English abstract).

Wang, D., Xu, H., Lin, J., and Hu, J.: Anticyclonic eddies in the northeastern South China Sea during winter 2003/2004, J. Oceanogr., 64, 925–935, 2008a.

Wang, G.: Discussion on the Movement of Mesoscale Eddies in the South China Sea, Ph.D. Dissertation, Ocean University of China, Qingdao, 2004.

Wang, G., Chen, D., and Su, J.: Winter eddy genesis in the Eastern South China Sea due to orographic wind jets, J. Phys. Oceanogr., 38, 726–732, doi:10.1175/2007JPO3868.1, 2008b.

Wang, G., Chen, D., and Su, J.: Generation and life cycle of the dipole in the South China Sea summer circulation, J. Geophys. Res., 111, C06002, doi:10.1029/2005JC003314, 2006.

Wang, G., Su, J., and Chu, P.: Mesoscale eddies in the South China Sea observed with altimeter data, Geophys. Res. Lett., 30(21), 2121, doi:10.1029/2003GL018532, 2003.

Wang, L., Koblinsky, C. J., and Howden, S.: Mesoscale variability in the South China Sea from the TOPEX/Poseidon altimetry data, Deep-Sea Res. I, 47, 681–708, 2000.

White, W. B.: Tropic coupled Rossby waves in the Pacific ocean-atmosphere system, J. Phys. Oceanogr., 30(6), 1245–1264, 2000.

Wu, C. and Chang, C. W. J.: Interannual variability of the South China Sea in a data assimilation model, Geophys. Res. Lett., 32, L17611, doi:10.1029/2005GL023798, 2005.

Wu, C. and Chiang, T.: Mesoscale eddies in the northern South China Sea, Deep-Sea Res. II, 54, 1575–1588, 2007.

Wu, C., Tang, T., and Lin, S.: Intra-seasonal variation in the velocity field of the northeastern South China Sea, Cont. Shelf Res., 25, 2075–2083, 2005.

Wyrtki, K.: Scientific results of marine investigation of the South China Sea and Gulf of Thailand, NAGA Report, 2, 195, 1961.

Xie, S., Xie, Q., Wang, D., and Liu, W.: Summer upwelling in the South China Sea and its role in regional climate variations, J. Geophys. Res., 108(C8), 3261, doi:10.1029/2003JC001867, 2003.

Xiu, P., Chai, F., Shi, L., Xue, H., and Chao, Y.: A census of eddy activities in the South China Sea during 1993–2007, J. Geophys. Res., 115, C03012, doi:10.1029/2009JC005657, 2010.

Xu, X., Qiu, Z., and Chen, H.: The general descriptions of the horizontal circulation in the South

China Sea, Proceedings of the 1980 Symposium on Hydrometeorology, Chinese Society of Oceanology and Limnology, Science Press, Beijing, 137–145, 1982.

Yang, K., Shi, P., Wang, D., and Qi, Y.: Numerical study about the mesoscale multi-eddy system in the northern South China Sea in winter, Acta Oceanol. Sinica, 22(1), 27–34, 2000 (in Chinese with English abstract).

Yasdi, R.: Combining rough sets learning and neural learning: method to deal with uncertain and imprecise information, Neuralcomputing, 7(1), 61–84, 1996.

Yuan, D., Han, W., and Hu, D.: Surface Kuroshio path in the Luzon Strait area derived from satellite remote sensing data, J. Geophys. Res., 111, C11007, doi:10.1029/2005JC003412, 2006.

Yuan, D., Han, W., and Hu, D.: Anti-cyclonic eddies northwest of Luzon in summer–fall observed by satellite altimeters, Geophys. Res. Lett., 34, L13610, doi:10.1029/2007GL029401, 2007.

Yuan, S. Y. and Wang, Z. Z.: Topography forced Rossby waves in the section from Xisha to Dongsha Islands, Trop. Oceanol., 5(3), 1–6, 1986 (in Chinese with English abstract).

Zhuang, W., Xie, S., Wang, D., Taguchi, B., Aiki, H., and Sasaki, H.: Intraseasonal variability in sea surface height over the South China Sea, J. Geophys. Res., 115, C04010, doi:10.1029/2009JC005647, 2010.

Table 1. Comparison of current speed derived from NLOM with cruise measurement.

Date	Long. (° E)	Lat. (° N)	U_{ADCP} (m s^{-1})	U_{NLOM} (m s^{-1})	δU (%)
2008/08/16	115.5819	21.9792	0.1972	–	–
2008/08/17	118.4670	22.0331	0.5448	0.3080	56.53
2008/08/18	119.8457	21.3517	0.4631	0.3385	73.09
2008/08/19	119.8736	19.0399	0.2419	0.2787	84.79
2008/08/20	116.3940	18.1005	0.3667	0.3430	93.54
2008/08/21	111.3139	17.3159	0.2210	0.2588	82.90
2008/08/22	110.2487	17.3391	0.1031	0.0870	84.38
2008/08/25	110.4957	18.0106	0.1632	–	–
2008/08/26	112.8241	18.0117	0.3036	0.4579	49.18
2008/08/27	116.5421	18.0086	0.3420	0.3385	98.98
2008/08/28	114.2493	18.0073	0.3153	0.4996	41.55
2008/08/29	111.5718	18.4941	0.2528	0.0750	29.67
2008/08/30	111.3114	18.9107	0.1194	–	–
2008/08/31	111.4607	19.2758	0.2247	–	–
2008/09/01	113.2634	19.5524	0.3714	0.2787	75.04
2008/09/02	115.8565	19.2557	0.2843	0.4996	24.27
2008/09/03	115.7976	20.0368	0.3054	0.1828	59.86
2008/09/04	117.0650	20.1009	0.2638	0.2172	82.34
2008/09/05	115.6592	20.4859	0.2232	0.1362	61.02
2008/09/06	113.8046	21.2015	0.1279	–	–

Table 2. Decision table constructed from the spatial-temporal relationships of mesoscale eddies in 4 zones of the SCS.

Condition attribute											Decision attribute
Time	Type	Intensity (m)	Vorticity ($\times 10^{-6}\,\mathrm{s}^{-1}$)	Horizontal scale (km)	CentralTemp (°)	TempDiff (°)	Distance relationship (km)	Directional relationship	Topological relationship	Mean depth (m)	Origin place
Winter	Warm eddy	0.09	0.7	151	23.31	0.03	77	East	Disjoint	2028	Z_2
Summer	Cold eddy	0.18	1.0	201	29.94	0.08	20	Southeast	overlapping	802	Z_4

Table 3. Decision table constructed from the spatial-temporal relationships of mesoscale eddies generated in 4 seasons.

Condition attribute											Decision attribute
Origin place	Type	Intensity (m)	Vorticity ($\times 10^{-5}\,s^{-1}$)	Horizontal Scale (km)	CentralTemp (°)	TimeDiff (°)	Distance relationship (km)	Directional relationship	Topological relationship	Mean depth (m)	Time
Z_1	Warm eddy	0.23	0.12	172	29.13	0.08	11	north	Overlapping	1757	autumn
Z_3	Warm eddy	0.12	0.07	196	28.65	1.42	26	northeast	overlapping	1712	winter

Table 4. Decision table constructed from the spatial-temporal relationships of the type of mesoscale eddies.

Condition attribute											Decision attribute
place Origin	Time	Intensity (m)	Vorticity ($\times 10^{-5}\,\mathrm{s}^{-1}$)	Horizontal Scale (km)	CentralTemp (°)	TimeDiff (°)	Distance relationship (km)	Directional relationship	Topological relationship	Mean depth (m)	Type
Z_2	Autumn	0.15	0.06	202	26.41	0.53	199	East	Disjoint	1645	Warm eddy
Z_1	autumn	0.27	0.11	194	28.58	0.23	43	East	overlapping	1903	Cold eddy

Table 5. Spatial-temporal rule extracted from the typical states of mesoscale eddies in 4 zones of the SCS.

No.	Spatial-temporal rule	Certainty level%	Coverage level %
1	Type(Cold Eddy) AND Vorticity ([0.7×10^{-6},*)) AND HorizontalScale ([*,173)) AND CentralTemp ([*,26.92)) => Zone (Z_1)	100	15.5
2	Time(Winter) AND Type(Cold Eddy) AND Vorticity ([0.7×10^{-6},*)) AND CentralTemp ([*,26.92)) => Zone(Z_1)	100	14.3
3	Type(Warm Eddy) AND Intensity ([*,0.08)) AND Vorticity ([*,0.7×10^{-6})) AND CentralTemp ([26.92,28.53)) => Zone(Z_3)	100	13.3
4	Time(Winter) AND Vorticity ([*, 0.7×10^{-6})) AND CentralTemp ([26.92,28.53)) => Zone(Z_3)	100	13.3
5	Time(Summer) AND HorizontalScale ([195,*)) AND Depth ([900, 2400]) => Zone(Z_4)	100	11.9

Note: "[ ]" represents the closed interval, "( )" the open interval, "*" the infinite interval, as follows.

Title Page
Abstract | Introduction
Conclusions | References
Tables | Figures
◂◂ | ▸▸
◂ | ▸
Back | Close
Full Screen / Esc
Printer-friendly Version
Interactive Discussion

Table 6. Spatial-temporal rule extracted from the typical states of mesoscale eddies in 4 seasons.

No.	Spatial-temporal rule	Confidence level (%)	Coverage Level (%)
1	Zone (Z_2) AND Type (Warm Eddy) AND Vorticity ([0.6×10^{-6}, *)) AND CentralTemp ([*, 26.22)) => Time (Winter)	100	32.5
2	Zone (Z_2) AND Type (Warm Eddy) AND CentralTemp ([*, 26.22)) AND TempDiff ([*, 0.18)) => Time (Winter)	100	20.8
3	Zone (Z_2) AND CentralTemp ([*, 26.22)) AND Depth ([500, 2800]) => Time (Winter)	100	20.8
4	CentralTemp ([*, 26.22)) AND TempDiff ([*, 0.18)) AND Depth ([500, 3000]) => Time (Winter)	100	20.0
5	Zone (Z_2) AND Type (Warm Eddy) AND HorizontalScale ([147, 190)) AND CentralTemp ([*, 26.22)) => Time (Winter)	100	18.3
6	Zone (Z_2) AND Vorticity ([0.06×10^{-6}, *)) AND CentralTemp ([*, 26.22)) AND Topology (overlapping) => Time (Winter)	100	17.5
7	Zone (Z_2) AND Type (Warm Eddy) AND CentralTemp ([*, 26.22)) AND Direction (Northeast) => Time (Winter)	100	14.2
8	Vorticity ([0.06×10^{-6}, *)) AND CentralTemp ([*, 26.22)) AND Topology (overlapping) AND Depth ([500, 4200)) => Time (Winter)	100	13.3
9	Zone (Z_2) AND Type (Warm Eddy) AND Intensity ([0.16, *)) AND CentralTemp ([26.22, 28.72)) => Time (Autumn)	100	11.7
10	Zone (Z_4) AND CentralTemp ([29.59, *)) AND Distance ([19, 42)) => Time (Summer)	100	11.6
11	Type (Warm Eddy) AND CentralTemp ([29.59, *)) AND TempDiff ([*, 0.18)) AND Depth ([2800, 4200]) => Time (Summer)	100	11.6

Title Page
Abstract | Introduction
Conclusions | References
Tables | Figures
◂| |▸
◂ ▸
Back | Close
Full Screen / Esc
Printer-friendly Version
Interactive Discussion

Table 7. Spatial-temporal rule extracted from the typical states of two types of mesoscale eddies.

No.	Spatial-temporal rule	Confidence level (%)	Coverage Level (%)
1	Vorticity ([*, 0.7×10^{-6})) AND CentralTemp ([29.02, *)) AND Distance ([*, 48)) => Type (Warm Eddy)	100	22.3
2	Vorticity ([*, 0.7×10^{-6})) AND CentralTemp ([29.02, *)) AND Temp ([*, 0.16)) => Type (Warm Eddy)	100	20.1
3	Intensity ([0.17, *)) AND Vorticity ([0.9×10^{-6}, *)) AND Depth ([1400, 2400]) => Type (Cold Eddy)	100	17.3
4	Time (Winter) AND Depth ([500,4400]) => Type (Warm Eddy)	100	16.3
5	Zone (Z_3) => Type (Warm Eddy)	100	15.9
6	Zone (Z_4) AND Intensity ([0.17, *)) AND Vorticity ([0.9×10^{-6}, *)) => Type (Cold Eddy)	100	15.3
7	Zone (Z_1) AND Vorticity ([0.9×10^{-6}, *)) AND Depth ([1000, 4200]) => Type (Cold Eddy)	100	14.3
8	Time (Autumn) AND Vorticity ([0.9×10^{-6}, *)) AND Depth ([500, 4200]) => Type (Cold Eddy)	100	14.3
9	Intensity ([*, 0.10)) AND CentralTemp ([29.02, *)) AND Distance ([*, 48)) => Type (Warm Eddy)	100	13.8
10	Vorticity ([0.9×10^{-6}, *)) AND CentralTemp ([27.72, 29.02)) AND Depth ([1000, 4000]) => Type (Cold Eddy)	100	13.3
11	Zone (Z_2) AND Time(Winter) AND Distance ([*, 48)) => Type (Warm Eddy)	100	12.4
12	CentralTemp ([*, 27.72)) AND Depth ([1200,3600]) => Type (Cold Eddy)	100	12.2
13	Time (Spring) AND Vorticity ([0.9×10^{-6}, *)) AND Topology (Disjoint) => Type (Cold Eddy)	100	11.2

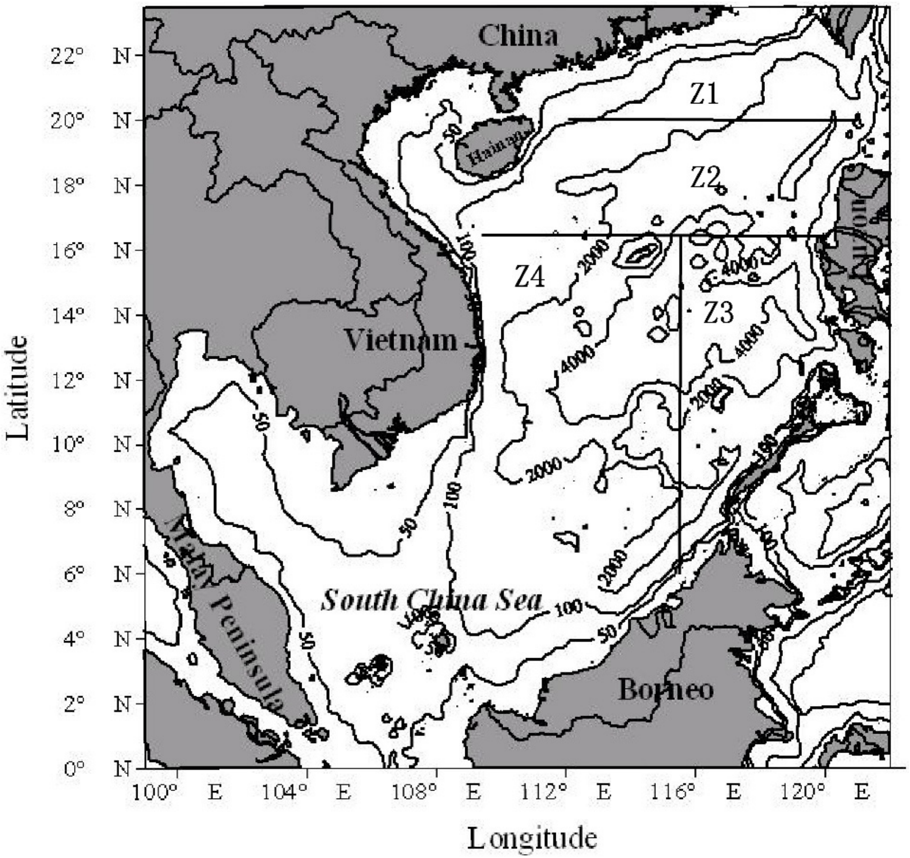

Fig. 1. Topography of the SCS (Z_1: northeastern SCS; Z_2: central SCS; Z_3: southeastern SCS; Z_4: southwestern SCS; Solid lines are the boundaries of Z_1, Z_2, Z_3 and Z_4).

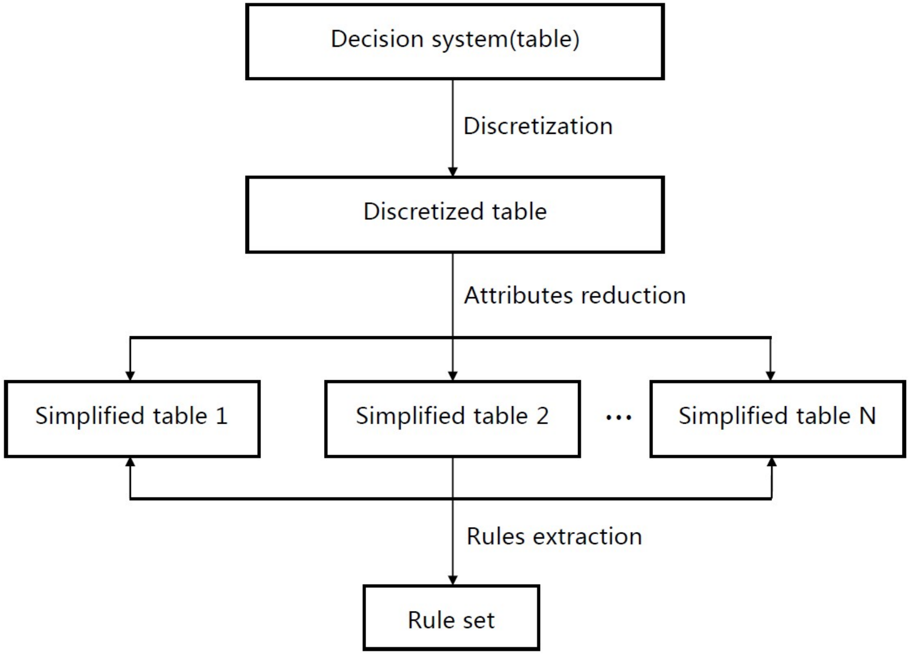

Fig. 2. Flowchart of the procedures to represent spatial-temporal relationships among mesoscale-eddy states.

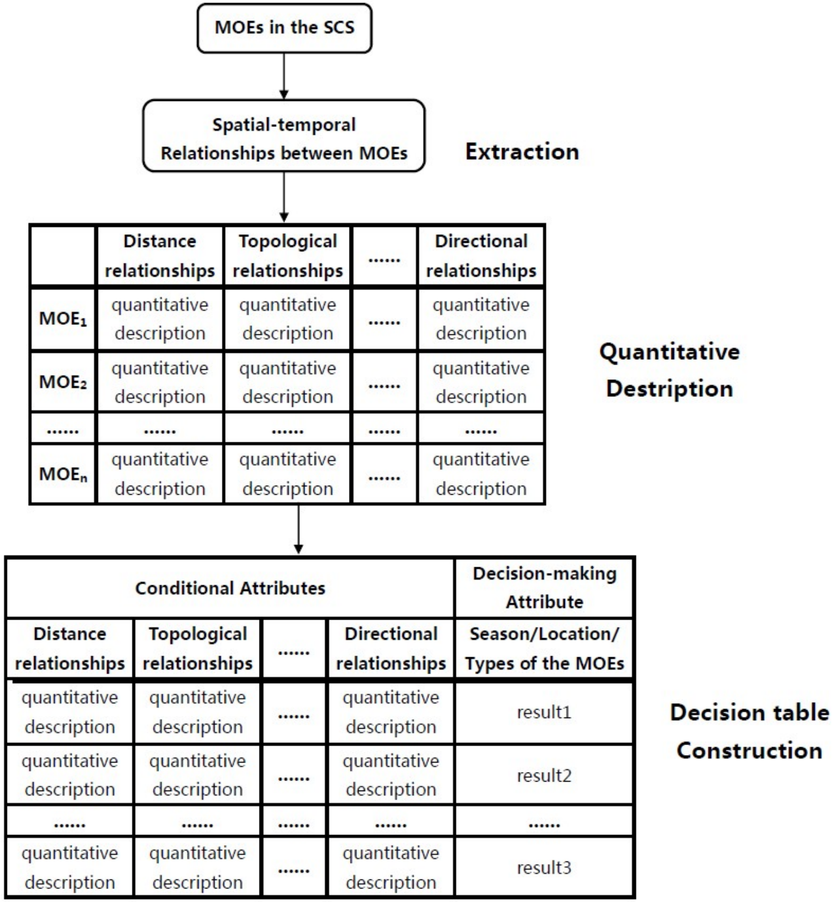

	Distance relationships	Topological relationships	......	Directional relationships
MOE₁	quantitative description	quantitative description	......	quantitative description
MOE₂	quantitative description	quantitative description	......	quantitative description
......	......	......	......	......
MOEₙ	quantitative description	quantitative description	......	quantitative description

Conditional Attributes				Decision-making Attribute
Distance relationships	Topological relationships	......	Directional relationships	Season/Location/ Types of the MOEs
quantitative description	quantitative description	......	quantitative description	result1
quantitative description	quantitative description	......	quantitative description	result2
......	......	......	......	......
quantitative description	quantitative description	......	quantitative description	result3

Fig. 3. Flowchart of major analysis steps based on the rough set theory.

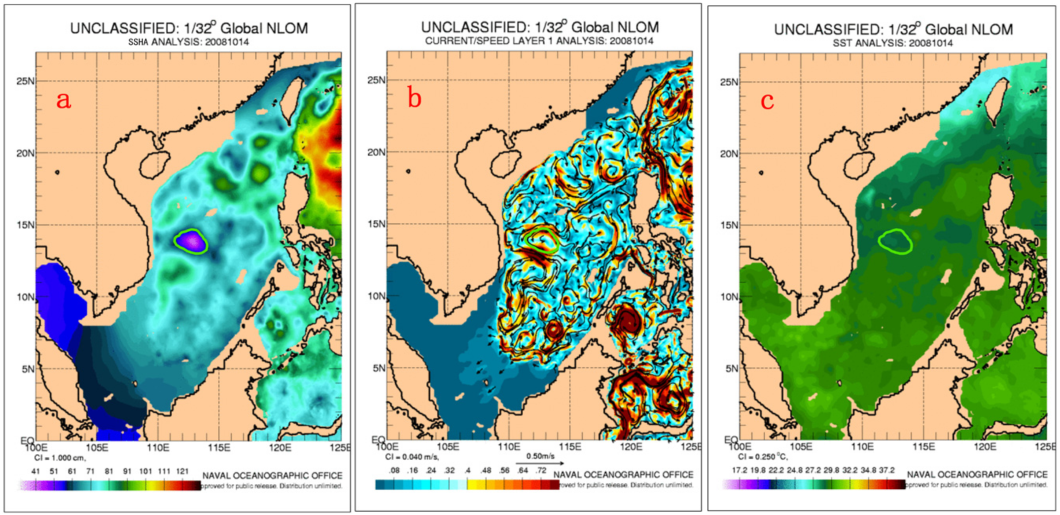

Fig. 4. Sketch map of a mesoscale eddy in the SCS (the corresponding raw datasets used to derive eddies are also shown in this figure).

Title Page
Abstract | Introduction
Conclusions | References
Tables | Figures
◀| |▶
◀ ▶
Back | Close
Full Screen / Esc
Printer-friendly Version
Interactive Discussion

Title Page
Abstract | Introduction
Conclusions | References
Tables | Figures
◀| |▶
◀ ▶
Back | Close
Full Screen / Esc
Printer-friendly Version
Interactive Discussion

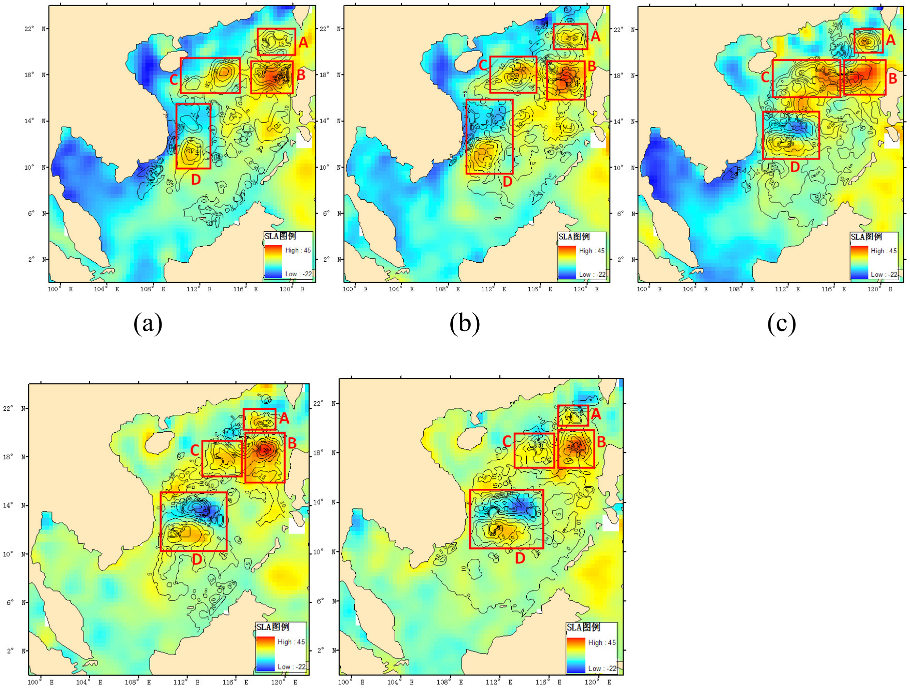

(a) (b) (c)

(d) (e)

Fig. 5. Spatial distribution of typical mesoscale-eddy states in the SCS extracted from Table 2 (red triangle, black square, green star, purple dot and yellow pentagon represent the states of eddy following rules 1–5 in Table 2, respectively. Blue line is 2000 m isobaths).

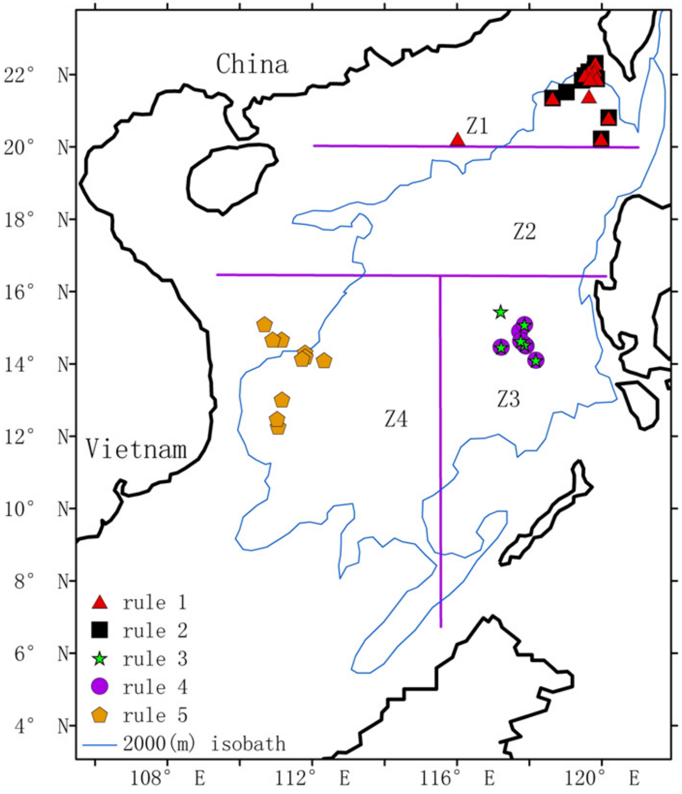

Fig. 6. Spatial distribution of typical mesoscale-eddy states in the SCS extracted from Table 5 red triangle, green star, purple dot yellow diamond and black square represent the states of eddy following rule 1, 3, 5, 10 and 11 in Table 3, respectively. Blue line is 2000 m isobaths).

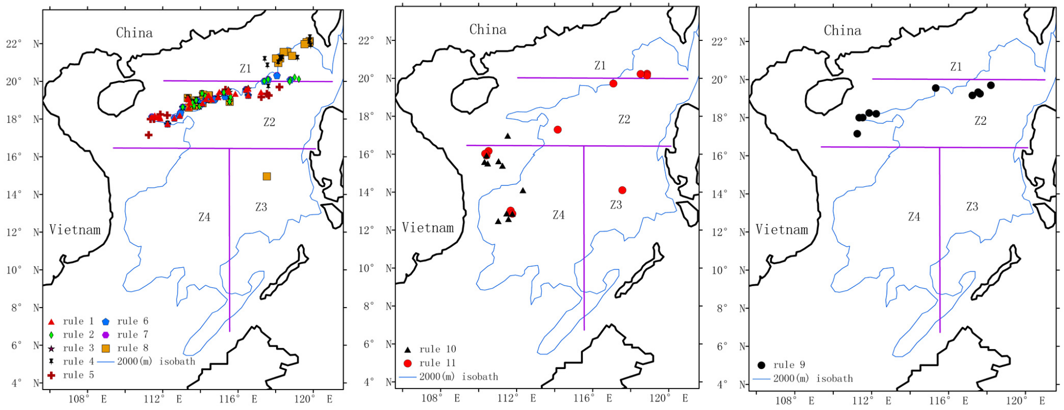

(a) winter (b) summer (c) fall

Fig. 7. Spatial distribution of typical states of the two types of mesoscale eddies in the SCS extracted from Table 6 with all states of cold eddies and warm eddies (red triangle and green dot represent the typical states of eddy following rule 1 and rule 3 in Table 4, respectively. Black pentagon and yellow square represent all typical states of cold eddies and warm eddies, respectively. Blue line is 2000 m isobaths).

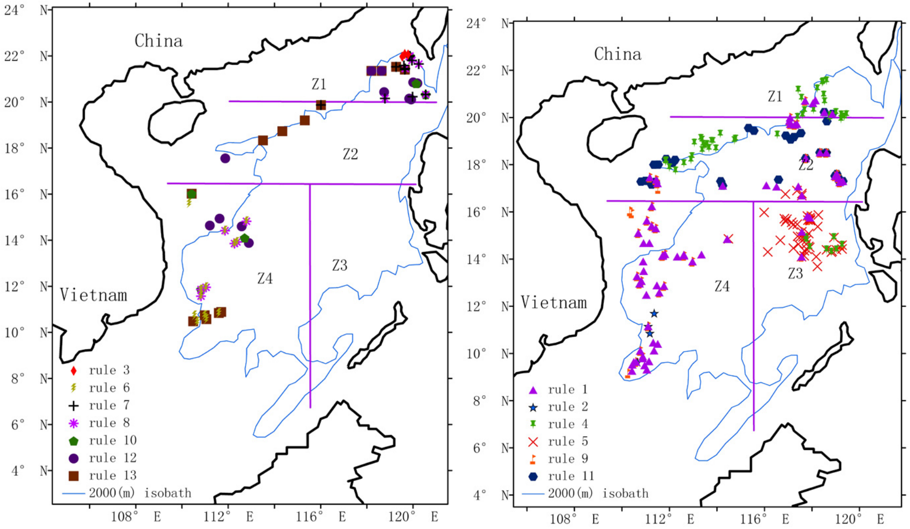

(a) cold eddies (b) warm eddies

Fig. 8. Spatial distribution of all typical cold-eddy states **(a)** and warm eddies **(b)** in the SCS extracted from Table 7 (blue line is 2000 m isobaths).

Title Page
Abstract Introduction
Conclusions References
Tables Figures
|◀ ▶|
◀ ▶
Back Close
Full Screen / Esc
Printer-friendly Version
Interactive Discussion